High Encoding Capacity Chipless RFID Tag

Milan Polivka [1], Milan Svanda [2]
[1] Dept. of Electromagnetic Field, Czech Technical University in Prague, FEE, Prague, Czech Republic, polivka@fel.cvut.cz

***Abstract*— In this work, we introduce a novel chipless RFID tag with high encoding capacity, which uses sub-band frequency shift coding (SB-FSC) to increase the number of bits encoded by each resonator. The tag consists of an array of *N* variable-length microstrip line resonators, each with up to $M = 9$ notches (corresponding to digits 0-9) to encode $N \times \log_2 M$ bits/tag. In addition, a pair of microstrip resonators serves as a frequency reference. A 60 × 80 mm² proof-of-concept tag is demonstrated with 13 + 2 resonant microstrip elements (for GTIN-13 code) to provide 43 bits/tag. The tag operates in the frequency range from 1.4 to 4.2 GHz with a coding density 36.7 bits/λ^2/GHz at the center frequency. The presented design thus enables the integration of chipless RFID technology with the GS1 standard systems and Internet of Things (IoT) paradigm.**

Index Terms*—chipless radio-frequency identification, EAN/GTIN encoding, electromagnetic scatterer, GS1 standard, Internet of Things, planar resonator, quality factor, radar cross-section, stripline resonator.

I. Introduction

Nowadays, chip RFID technology is widespread in industry, logistics, entertainment and other applications [1] and is thus well-integrated within the Internet of Things (IoT) paradigm. However, there are still many unsolved complexities in RFID applications, such as identifying tags placed in close proximity of lossy dielectric or metallic objects [2] or people [3-5], as well as the development of sensing RFID tags [6, 7].

A recent trend in RFID [8] is based on obtaining identification information without the use of semiconductor chips (*chipless* RFID), which promises to further reduce the complexity and cost of transponders. In addition to this undeniable advantage, this technology does present a number of challenges that must be thoroughly addressed in order to use these systems reliably and efficiently. Among others, these include predominantly maximization comprehensive encoding capacity related to the relative electrical size of the transponder and to the unit bandwidth (bits/λ^2/GHz) [9].

Several solutions have been proposed to design high-capacity transponders [10-13]. Among them include a frequency shift coding (FSC) that applies fine frequency tuning of each resonator within sub-bands such as a series of planar ring resonators [14] or different length strip resonators with a step change in the characteristic impedance [15]. However, these solutions exhibit low spatial-spectral encoding density.

We introduce a novel chipless RFID tag with high encoding capacity, which uses sub-band FSC (SB-FSC) to increase the number of bits encoded by each resonator. The tag consists of an array of N variable-length microstrip line resonators, each with up to $M = 9$ notches (corresponding to digits 0-9) to encode $N \times \log_2 M$ bits/tag. In addition, a pair of microstrip resonators serves as a frequency reference. A proof-of-concept tag is demonstrated with 13 + 2 resonant microstrip line elements (for GTIN-13 code) backed by a metallic plate to provide 43 bits/tag. The proposed solution thus enables the integration of chipless RFID technology with the GS1 standard systems and Internet of Things (IoT) paradigm.

II. Tag Design

The tag consists of 15 strip elements with the lengths in the interval {25.36, 26.66, 27.82, 29.45, 31.28, 33.35, 35,70, 38.41, 41.56, 45.27, 49.67, 55.05, 59.69, and 2× 22.38} mm, a strip width ranging from 1.5 to 3.0 mm, and a gap of 1 mm between 13 strips, etched on a 1.524 mm thick Astra MT77 dielectric substrate ($\varepsilon_r = 3.0, \tan\delta = 0.0017$) backed by a 60 × 80 mm² metallic plate; see Fig. 1.

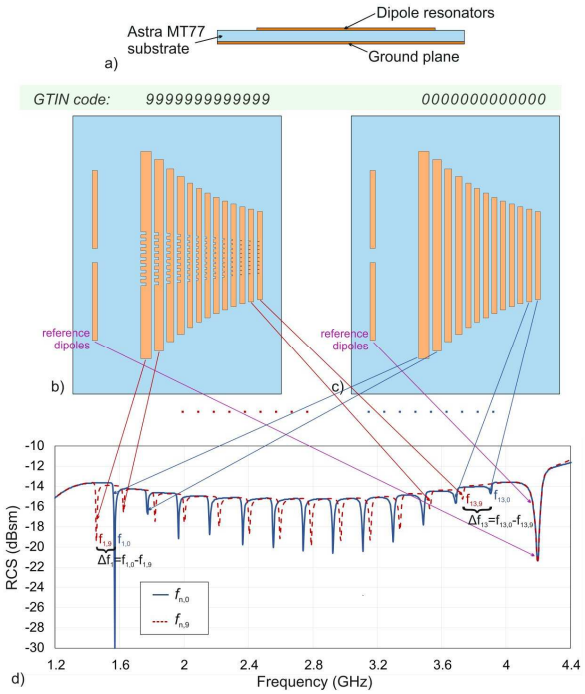

Fig. 1. Chipless RFID tags using sub-band frequency shift coding (SB-FSC) of inner thirteen dipole scatterers to implement EAN/GTIN-13 codes: a) 0000000000000, b) 9999999999999. Corresponding frequency response of the RCS(f) curve where minima on a dashed line represent local reference frequencies $f_{1,0}$ to $f_{13,0}$ (code 0000000000000) and minima on a solid line represent frequencies $f_{1,9}$ to $f_{13,9}$ (code 9999999999999) are depicted in c).

The 13 elements are used to encode the digits of the GTIN-

13 code, and the pair of left-hand elements serve as the system reference. The tag operates in the frequency range from 1.4 to 4.2 GHz with an encoding capacity of 36.7 bits/λ^2/GHz at the center operating frequency evaluated with respect to the relative electrical size of the tag and the frequency range used.

A. Operational Principle

In a basic tag arrangement, an array of 13 smooth strips resonates on 13 local reference frequencies $f_{n,0}$, where n is the natural number from the interval {1; 13}, and corresponds to GTIN-13 code '0000000000000'; see Fig. 1 and Fig. 2.

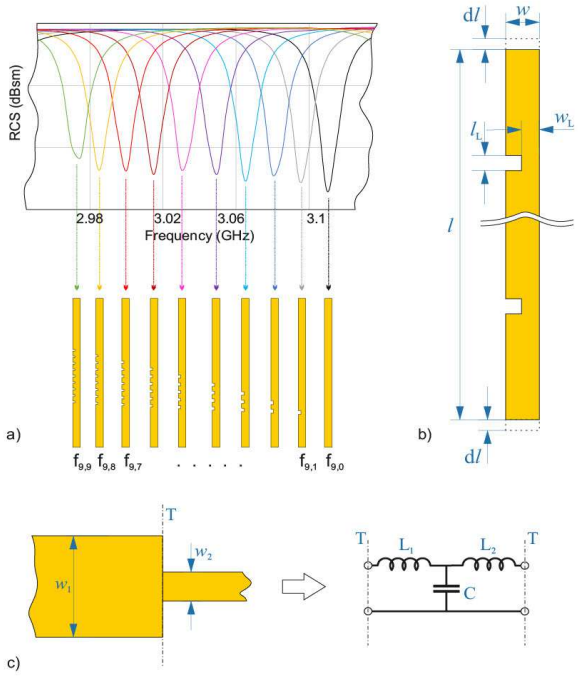

Fig. 2 a) Simulated frequency shift df of the resonance minima on the RCS curve corresponding to one grounded strip element loaded with no to nine notches, b) sketch of the strip loaded by notches treated as TL resonator, c) sketch and equivalent circuit model of microstrip step discontinuity at the junction of two lines of different widths.

Encoding of digits 1-9 at each of the n positions of GTIN code is achieved by fine frequency shift $df_m = m*df$ of strip-scatterers from their corresponding local reference frequency $f_{n,0}$ to frequencies $f_{n,m} = f_{n,0} - df_m$ within dedicated frequency sub-bands $\Delta f_n = f_{n,9} - f_{n,0}$ where m = 1, 2, .., 9 represents one of the digits 1-9; see Fig. 2a). The relationship $f_{n,m} < f_r$ holds for the system reference frequency f_r in the proposed design. However, $f_r < f_{n,m}$ is also possible if the reference resonator is placed next to the shortest element to reduce mutual coupling with the largest digit-coding elements. The frequency shift df_m of digit-coding elements from their local reference frequencies $f_{n,0}$ within dedicated frequency sub-bands Δf_n is achieved by appropriately segmenting their perimeters with one to nine single-sided notches. Such structuring of the central part of the strip extends the length of the resonant current waveforms and provides necessary frequency shifts; see Fig. 2a). A simulation of an electromagnetic tag showing the RCS curve of all the same 13-digit words is shown in Fig. 2. Each of the minima can be found in its tolerance frequency band df_{tol}, which is found to be 16 MHz for simulation; see Fig. 4b). Unlike chipless RFID tags using the presence/absence of coding elements to encode bit "1" or "0", e.g. [12], [13], which usually suffer from unwanted frequency detuning and amplitude distortion due to the coupling between the elements when zero bits are coded (appropriate elements are removed), the proposed method doesn't remove bit-coding elements and it is thus more robust to these undesirable effects.

B. Single Element Design

Frequency response of a single strip element with none to nine notches and a corresponding frequency shift df of the resonance minimum on the RCS curve within a dedicated sub-band Δf_n is depicted in Fig. 2a). Due to a different thickness coefficient (relative length-to-width dimensions) of the strips in an array the same frequency shift at higher frequencies (for fixed strip width) is achieved by narrower and shallower notches as can be seen in Fig. 1b). That's why the notch width changes from 0.83 mm to 0.13 mm and the notch depth from 1.5 to 0.55 mm for longer to shorter strips, respectively.

The smooth strip metal backed element is considered as an open-circuit $\lambda_g/2$ microstrip transmission line (TL) resonator, whose resonant condition is given by $\beta_g l_{eff} = \pi$, where λ_g is a guided wavelength, β_g is the phase constant of the TL of the width w. The effective electrical length l_{eff} is given as $l_{eff} = L + 2dl$, where dl is the line extension due to fringing electric field at the open ends given by [16] as

$$dl = 0.412h \frac{\varepsilon_{eff}{}^{w} + 0.3}{\varepsilon_{eff}{}^{w} - 0.258} \frac{w/h + 0.264}{w/h + 0.8} \qquad (1)$$

The relation holds for $w/h \geq 0.2$ and $2 \leq \varepsilon_r \leq 50$ with an error < 4 %. Once the TL resonator is notched the effective length l_{eff} is extended due to the phase delay caused by each step discontinuity at the interfaces of the difference strip widths, see Fig. 2b). The phase resonant condition of the notched TL resonator is expressed as

$$\beta_L n l_L + \beta_g (l - n l_L) + 2dl + 2nd\Psi = \pi \qquad (2)$$

where β_L is a phase constant of the short narrow stub of the length $l_L = n_w$ and the width $w_L = w - n_d$ formed by a stub of notched strip TL; see Fig. 3b), n_w is the notch width, n_d is the notch depth, and n is the number of notches. β_g is a phase constant of the original unnotched strip TL of the width w, $2dl$ is a length extension due to fringing fields at the open strip ends, $d\Psi$ is a phase extension due to time delay t_D caused by parasitic LC elements of the equivalent circuit model of the step discontinuity at the interface of TLs of the different strip widths. Phase extension $d\Psi = kTL\Delta l = 2\pi/\lambda_g v_p t_D = 2\pi c t_D/\lambda_g$ is given by time delay $t_D = \sqrt{LC}$ according to [17].

III. MEASUREMENT

To verify the properties of the proposed transponders, we performed monostatic measurements of tag RCS response by utilizing a Rohde & Schwarz ZVA 40 network analyzer within the frequency band of 1.0 to 4.5 GHz in an anechoic chamber; see Fig 3. The measurements were based on the evaluation of the reflection coefficient of a double ridge horn antenna DRH20 [18] in front of which a transponder was placed at a distance of 25 cm.

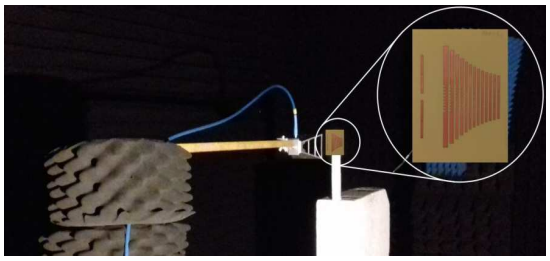

Fig. 3 Measurement setup using monostatic configuration in an anechoic chamber with the tag detail.

The measured transponder RCS response; see Fig. 4, is performed using the following relation [13]:

$$\sigma_{\mathrm{tag}} = 20 \log \frac{\left|S_{11}^{\mathrm{tag}} - S_{11}^{\mathrm{iso}}\right|}{\left|S_{11}^{\mathrm{ref}} - S_{11}^{\mathrm{iso}}\right|} \sigma_{\mathrm{ref}}, \tag{3}$$

where $S_{11}{}^{\mathrm{tag}}$ is the reflection coefficient, provided that the measured tag is used as a scatterer. $S_{11}{}^{\mathrm{ref}}$ represents the reflection coefficients, when the reference plate is used as a scatterer. $S_{11}{}^{\mathrm{iso}}$ is the reflection coefficient of the antenna itself in the case where no scatterer is used, which takes into account the residual reflection from experimental surroundings. σ_{tag} is the measured tag RCS, σ_{ref} represents the RCS of the reference scatterer, a rectangular metallic plate of a × b mm^2 in size and 0.3 mm in thickness, whose analytical formula is given by [19]

$$\sigma_{\mathrm{ref}} = 4\pi \frac{a^2 b^2}{\lambda^2}. \tag{4}$$

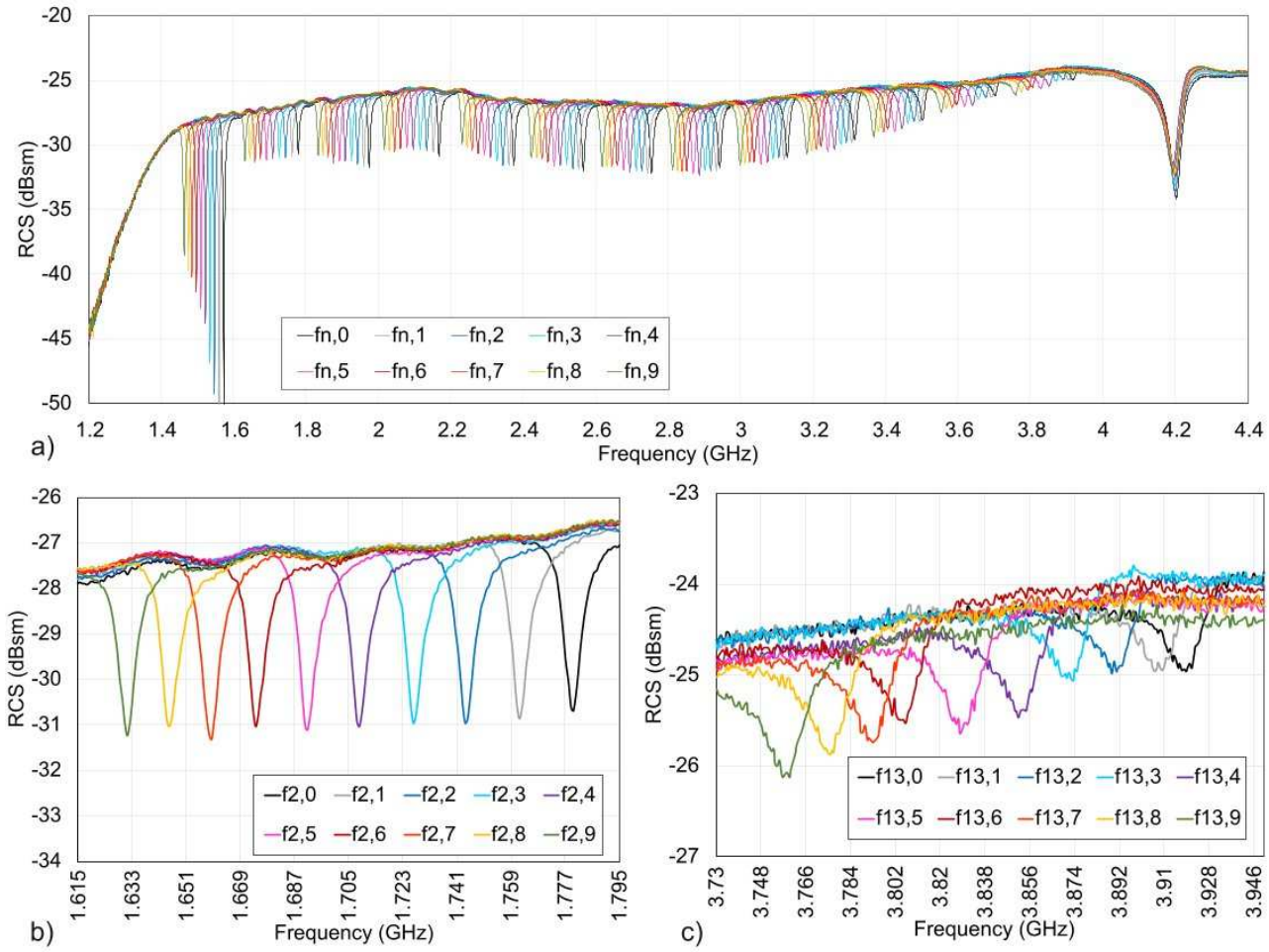

Fig. 4 Measured RCS curves for RFID tags with none to 9 notches introduced: a) in each of the 13 elements, i.e. each curve represent one of the 13 codes with the same digits (0000000000000 to 9999999999999), and b) in the second resonator representing frequency sub-band Δf_2, and c) last resonator representing the frequency sub-band Δf_{13}; the measured tolerance band is $\mathrm{d}f_{\mathrm{tol}} = 18$ MHz.

IV. COMMENTS

The simulated (Fig. 1) and measured (Fig. 4) values of RCS response of the proposed tags lead to the following observations:

The resonance minima depth of the scatterers on the RCS curve decreases with increasing frequency; see Fig. 4.

Each digit-coding strip element represents $\log_2 10 = 3.32$ bits resulting in a total $13 \times 3.32 = 43$ bits/tag which provides encoding density 36.7 bits/λ^2/GHz at the center of the operating frequency band 1.4 to 4.2 GHz.

The size of the longest strip elements, resonating at the lowest frequency, is designed for the minimum RCS response. The higher the frequency, the smaller the relative size of the strip scatterer compared to the backed metal plate, resulting in a larger deviation from the minimum reflection coefficient condition causing relatively shallow resonance minima on RCS curve; see Fig. 4a).

The measured frequency shift of a pair of the reference scatterers located at $f \approx 4.20$ GHz changes by approximately 8 MHz from 4.202 GHz to 4.194 GHz when 0 and 9 notches are introduced, respectively, which corresponds to a relative frequency change of 0.2 %.

Each of the minima on the RCS curve corresponding to a resonator with 0 to 9 notches can be found in its tolerance band $\mathrm{d}f_{\mathrm{tol}}$, which is, for example, 18 MHz for the measured results in the case of the second largest strip; see Fig. 4b).

The measured frequency shift of each resonant frequency $f_{\mathrm{n,m}}$ from the center of the appropriate tolerance band Δf_{n}; see Fig. 4b) and 4c), is also affected by slight changes of effective permittivity of the strip resonator considered as a microstrip TL line stub.

V. CONCLUSION

We introduce a novel chipless RFID tag that uses SB-FSC of each of the digit-coding elements, which is achieved by segmenting their perimeters with a set of single-sided notches that cause a shift in their resonant frequencies. A proof-of-concept tag is presented with $N = 13$ high quality factor resonant strip elements each capable of encoding a total of $M = 10$ digits providing 43 bits/tag and 36.7 bits/λ^2/GHz.

Unlike the frequency coding methods used in frequency domain chipless RFID technology, which utilize the presence or absence of a coding element representing a bit "1" or "0", respectively, the proposed method does not remove bit coding elements. The reading is thus more robust to undesirable effects caused by the mutual coupling among elements.

ACKNOWLEDGMENT

This work was supported by the Czech Science Foundation (project GA23-07518S) and the Ministry of Education, Youth and Sports of the Czech Republic (Program INTER-EXCELLENCE, Subprogram INTER-COST, Project LTC20012) and the COST – European Cooperation in Science and Technology (COST Action CA18223 SyMat).

REFERENCES

[1] K. Finkenzeller and D. Muller, RFID Handbook: Fundamentals and Applications in Contactless Smart Cards, Radio Frequency Identification and Near-Field Communication. John Wiley & Sons., 2010, p. 480.

[2] A. A. Babar, T. Bjorninen, V. A. Bhagavati, L. Sydanheimo, P. Kallio, and L. Ukkonen, "Small and Flexible Metal Mountable Passive UHF RFID Tag on High-Dielectric Polymer-Ceramic Composite Substrate," IEEE Antennas and Wireless Propagation Letters, vol. 11, pp. 1319-1322, 2012.

[3] G. Marrocco, "RFID Antennas for the UHF Remote Monitoring of Human Subjects," IEEE Transactions on Antennas and Propagation, vol. 55, no. 6, pp. 1862-1870, 2007.

[4] M. Svanda and M. Polivka, "Novel Dual-Loop Antenna Placed over Patch Array Surface for UHF RFID of Dielectric and Metallic Objects," Microwave and Optical Technology Letters, vol. 51, no. 3, pp. 709-713, Mar 2009.

[5] M. Svanda, M. Polivka, and P. Hudec, "Novel low-profile foam dielectric over-the-shoulder antenna based on coupled patches technique," Microwave and Optical Technology Letters, vol. 55, no. 3, pp. 593-597, Mar 2013.

[6] J. Kracek, M. Svanda, M. Mazanek, and J. Machac, "Implantable Semi-Active UHF RFID Tag With Inductive Wireless Power Transfer," IEEE Antennas and Wireless Propagation Letters, vol. 15, pp. 1657-1660, 2016.

[7] C. Occhiuzzi, S. Caizzone, and G. Marrocco, "Passive UHF RFID antennas for sensing applications: Principles, methods, and classifcations," IEEE Antennas and Propagation Magazine, vol. 55, no. 6, pp. 14-34, 2013.

[8] C. Herrojo, F. Paredes, J. Mata-Contreras, and F. Martín, "Chipless-RFID: A Review and Recent Developments," Sensors, vol. 19, no. 15, p. 3385, 2019.

[9] M. Svanda, M. Polivka, J. Havlicek, J. Machac, and D. H. Werner, "Platform Tolerant, High Encoding Capacity Dipole Array-Plate Chipless RFID Tags," IEEE Access, vol. 7, pp. 138707-138720, 2019.

[10] M. Added, N. Boulejfen, M. Svanda, F. M. Ghannouchi, and T.-P. Vuong, "High-Performance Chipless Radio-Frequency Identification Tags: Using a slow-wave Approach for miniaturized structure," IEEE Antennas and Propagation Magazine, vol. 61, no. 4, pp. 46-54, 2019,.

[11] O. Rance, R. Siragusa, P. Lemaitre-Auger, and E. Perret, "Toward RCS Magnitude Level Coding for Chipless RFID," IEEE Transactions on Microwave Theory and Techniques, vol. 64, no. 7, pp. 2315-2325, 2016.

[12] M. Svanda, J. Havlicek, J. Machac, and M. Polivka, "Polarisation independent chipless RFID tag based on circular arrangement of dual-spiral capacitively-loaded dipoles with robust RCS response," IET Microwaves, Antennas & Propagation, vol. 12, no. 14, pp. 2167-2171, 2018.

[13] A. Vena, E. Perret, and S. Tedjini, "A Fully Printable Chipless RFID Tag With Detuning Correction Technique," IEEE Microwave and Wireless Components Letters, vol. 22, no. 4, pp. 209-211, 2012.

[14] A. Vena, E. Perret, and S. Tedjini, "High-Capacity Chipless RFID Tag Insensitive to the Polarization," (in English), Ieee Transactions on Antennas and Propagation, vol. 60, no. 10, pp. 4509-4515, Oct 2012,.

[15] C. M. Nijas et al., "Low-Cost Multiple-Bit Encoded Chipless RFID Tag Using Stepped Impedance Resonator," IEEE Transactions on Antennas and Propagation, vol. 62, no. 9, pp. 4762-4770, 2014.

[16] R. Garg and I. J. Bahl, "Microstrip Discontinuities," Int. J. Electron., vol. 45, no. 1, p. 7, 1978.

[17] P. C. Magnusson, G. C. Alexander, V. K. Tripathi, and A. Weisshaar, Transmision Lines and Wave Propagation, 4th ed. CRC Press, 2001.

[18] "DRH20 - Double ridge waveguide horn." RFspin s.r.o. http://www.rfspin.cz/en/antennas/dual-polarized-antennas/drh20 (accessed 20.6., 2022).

[19] M. A. Richards, J. A. Scherr, and W. A. Holm, Eds., Principles of Modern Radar: Basic Principles. Rijeka, Croatia: SciTech, 2010.